Study of a 200 ton Gadolinium-loaded Water Cherenkov Detector for Super-KamiokaNDE Gadolinium Project

Chenyuan Xu
Okayama University
Student Num 41426209

Abstract

Supernova Relic Neutrino (SRN) has not been observed yet because of its low event rate and high background. By adding gadolinium into water Cherenkov detector, inverse beta decay will have two signals, the prompt one is positron signal and the delayed one is a ∼8 MeV gamma cascade from neutron capture on gadolinium. By this way, background for SRN can be largely reduced by detecting prompt and delayed signals coincidently, and Super-K will also have the ability to distinguish neutrino and anti-neutrino. SK-Gd is a R&D project proposed to dissolve gadolinium into Super-K. As a part of it, EGADS, a 200ton water Cherenkov detector was built in Kamioka mine. 0.2% gadolinium water has been successfully loaded into EGADS tank and the neutron capture efficiency of gadolinium in EGADS was measured to be
$Eff_{Gd}(Data) = 84.36 \pm 1.79\%$
$Eff_{Gd}(MC) = 84.51 \pm 0.33\%$
Current status of SK-Gd project and the physics work being performed in EGADS as well as the details of EGADS detector calibration and data analysis will be presented in this thesis.

Contents

1 Supernova neutrino

1.1 Supernova explosion

On February 23rd 1987, supernova burst of Large Magellanic Cloud was observed. It is a supernova from about 51.4kpc distance from the earth and it is numbered with SN1987A. It is the first time that human detected the supernova by neutrinos and that is the sign of the birth of Neutrino Astronomy. In SN 1987A, the neutrino detector KamiokaNDE observed 11 neutrinos [1], while American detector IBM observed 8 neutrinos [2]. The detection of supernova neutrino is not only a new page in the physics history but also proved that the fundamental model of core collapse supernova is correct. Study about supernova was based on optical observation in the past and it is limited by a lot of reasons. Neutrino has offered a new way to approach to the the mechanism of supernova explosion and cosmic evolution. Now experiments of supernova neutrino search are being carried out in the world wide.

Figure 1: Supernova 1987A

1.1.1 Time evolution of stellar

Supernova explosion is the last stage of the life of large stars. The last process of the stellar evolution depends on its mass.

Protostar : $M < 0.08 M_{\odot}$
The core of protostar is formed by the interstellar gases. The core will continue to absorb the nearby gases and grow larger and larger. The kinetic energy of the absorbed matter will be transferred to thermal energy and that is why protostar is brighter than the main sequence star. The Hydrogen in the core will not start to fuse until the core temperature reaches 10^7K. If the core begins to cool down before it reaches 10^7K, the Hydrogen will never begin to burn and the star will

finally become a black dwarf.
Jupiter is an example for protostar.

Hydrogen burning : $0.08M_\odot < M < 0.46M_\odot$
Hydrogen burning starts from $0.08M_\odot$. The reactions of Hydrogen burning is complex but the most basic one is:

$$4p \rightarrow^4 He + 2e^+ + 2\nu \tag{1}$$

Hydrogen supplies the energy and then the star could make balance from the temperature and inner pressure of itself. Star with mass less than $0.46M_\odot$ will stop burning its energy in this phase and then become a white dwarf which consists of Helium. The white dwarf will continue to emit light until it has completely cooled down and become a black dwarf. However, the life time of white dwarf is so long that it is even longer than the age of our current cosmic. So there is no black dwarf existing yet.

Helium burning : $0.46M_\odot < M < 4M_\odot$
When the Hydrogen burning stops, the star will begin to contract because of its gravitation. If the core temperature exceeds 10^8K, Helium will start to burn and finally becomes a red giant with a core of Carbon and Oxygen. As the size of the star increases, the gravitation in the penumbra becomes weak and the star begin to blast off the matter of its outside part. The core will remains and become a white dwarf. Our sun is an example for this.

Carbon deflagration : $4M_\odot < M < 8M_\odot$
For the stars whose mass is between $4M_\odot$ and $8M_\odot$, the Carbon-Oxygen core produced in the last process will begin to burn. The mass of the core is near the Chandrasekhar Limit and the degenerate pressure of the electrons is stronger. Thus, even though the core is burning, it could not expand and it is called Carbon deflagration. This is the mechanism of one type of supernova. When the core burns up, the total energy it gives out is even larger than the binding energy of the star so nothing could remain after the burst.

Gravitational collapse : $8M_\odot < M$
For the stars $8M_\odot < M < 12M_\odot$, Ne-Mg cores could be made by carbon burning under the degenerate pressure. And for the stars $12M_\odot < M$, iron core can be made and the core could not burn any more as iron is the most stable element. The core loses the source of energy and the temperature and pressure increase as the star contracts by gravitation. In the end, the star will die with a supernova explosion.

1.1.2 Neutrino reaction in supernova process

The process of supernova explosion can be divided as follows.

Beginning of core collapse
When the mass of the core exceed the Chandrasekhar Limit, the gravitational collapse will start and the density of the core will get larger and larger. ν_e will

be released by electron capture(2) by the nuclei and the photodisintegration of iron nuclei(3) also occurs in this step.

$$e^- + A(N,Z) \rightarrow \nu_e + A(N+1, Z-1) \tag{2}$$

$$\gamma + ^{56} Fe \rightarrow 13\alpha + 4n - 124.4MeV \tag{3}$$

Both of the two interactions will reduce the degenerate pressure and become the trigger of a rapid core collapse.

Neutrino trapping
When the density of the core exceeds $3 \times 10^9 g/cm^3$, the neutrinos will follows the coherent scattering(4) with the nuclei and be unable to go outside. This is called neutrino trapping and the boundary is called neutrino sphere.

$$\nu + A(N,Z) \rightarrow \nu + A(N,Z) \tag{4}$$

Core bounce
When core density continue to increase and finally reaches the level of nuclear density($\sim 10^{14} g/cm^3$), the shock wave will be repulsed and driven towards outside.

Neutrino cooling
After the shock wave passed through, the matter outside the core will drop to the center and $\sim 10^{53}$erg of gravitational energy will be converted into thermal energy. All flavors of neutrinos will be produced by pair annihilation(5) and bremsstrahlung(6).

$$e^- + e^+ \rightarrow \nu + \bar{\nu} \tag{5}$$

$$N + N \rightarrow N + N + \nu + \bar{\nu} \tag{6}$$

$\bar{\nu}_e$ and ν_e will also be produce by electron capture(7) and positron capture(8).

$$e^- + p \rightarrow \nu_e + n \tag{7}$$

$$e^+ + n \rightarrow \bar{\nu}_e + p \tag{8}$$

Most of the energy are released by neutrinos and the star cools down in about 10s.

Supernova burst
The shock wave may takes several hours until it arrives the surface of the star. The penumbra part will be blasted off and the remnant of the star will become neutron star. Or if the mass of the core is heavy enough, it will finally become a black hole.

Summarizing this session, only ν_e can be emitted in the very beginning of supernova explosion, and later after that neutrinos of all flavors will be produced.

1.2 Supernova Relic Neutrino

As 99% of the energy is released by neutrino flux in supernova process, it is an important way to study supernova models by neutrinos. It is considered that supernova occurs two or three times within one century in our galaxy [3]. Although there is no supernova observed from SN1987A, supernova is always occurring in the 15 billion years history of the universe. These neutrinos from past supernovae are called Supernova Relic Neutrinos (SRN), or known as another name as Diffuse Supernova Neutrino Background (DSNB). The first models for SRN were founded even before SN1987A [4], while the studies about SRN largely increased after SN1987A. Figure 2 shows the $\bar{\nu}_e$ fluxes predicted by the following theoretical models:

Constant SN rate model [5] (Totani et al. 1995)
The supernova rate was assumed as a constant in the whole universe in this model.

Population synthesis [6] (Totani et al. 1996)
It is founded by the same author by using a population synthesis of the stars in the galaxy evolution.

Cosmic gas infall model [7] (Malaney et al. 1997)
This model uses the supernova rate which is obtained from the density distribution of interstellar gas as a function of red shift parameter.

Chemical evolution model [8] (Hartmann et al. 1997)
This model considered the history of the cosmic star formation which is obtained from the chemical evolution.

Heavy metal model [9] (Kaplinghat et al. 2000)
In this model, the theoretical upper limit of SRN flux is predicted by using the abundance of heavy elements.

LMA neutrino oscillation [10] (Ando et al. 2002)
The parameter for neutrino oscillasion is considered in this model.

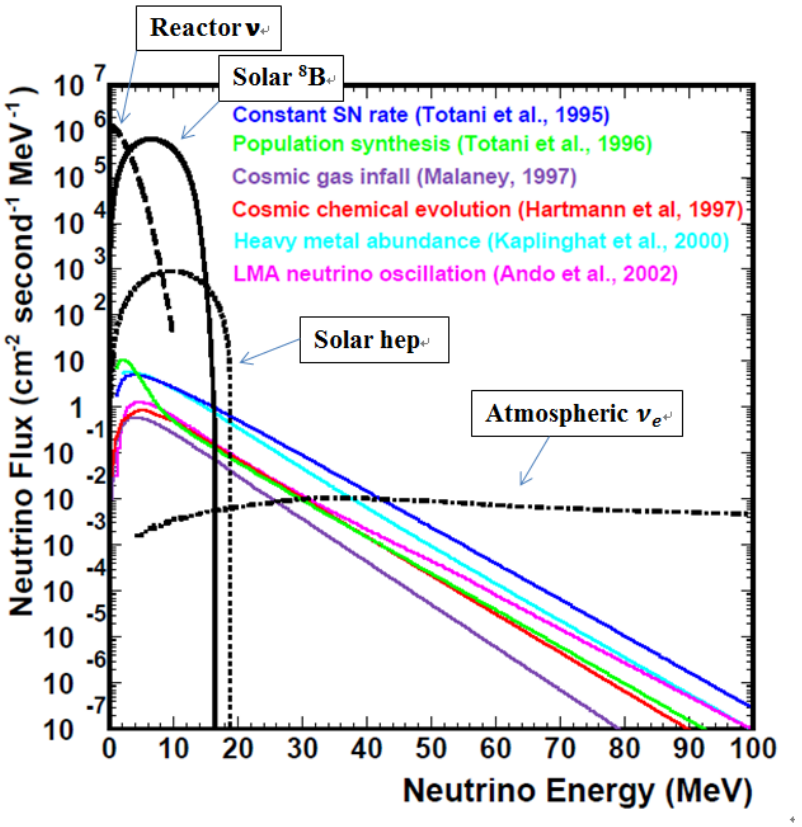

Figure 2: Colour lines are the $\bar{\nu}_e$ flux predicted by each model. Black lines represent other background neutrinos.

The reason why only $\bar{\nu}_e$ is considered is that the cross section of $\bar{\nu}_e$ reaction in water Cherenkov detector is two orders larger than the others in the main energy range of SRN. Even though $\bar{\nu}_e$ reaction has large cross section, SRN flux is still hidden in various background and has not been detected yet. As can been seen from the Figure 2, Solar and reactor neutrinos are dominant below 10MeV, and atmospheric neutrinos become dominant above 30MeV. A new R&D project focusing on SRN search in 10∼30MeV window is now being carried out. The details will be stated later.

2 Super-Kamiokande detector

2.1 Super-K Detector overview

Super-K, which is short for Super-KamaiokaNDE, is a neutrino detector built in 1000m underground in Kamioka mine in Gifu Prefecture of Japan. The last three letters NDE means neutrino detection experiment as well as nucleon decay experiment. It is a water Cherenkov detector as a stainless cylinder of 39m radius and 42m height, with total volume of 50000 tons water. The rock around the detector acts as a shield to stop the comic muons and other kinds of backgrounds from environment like gamma rays and neutrons. However, due to the small cross section of neutrino reactions, neutrino can easily even go through the earth and it is also the reason for the large volume of water target.

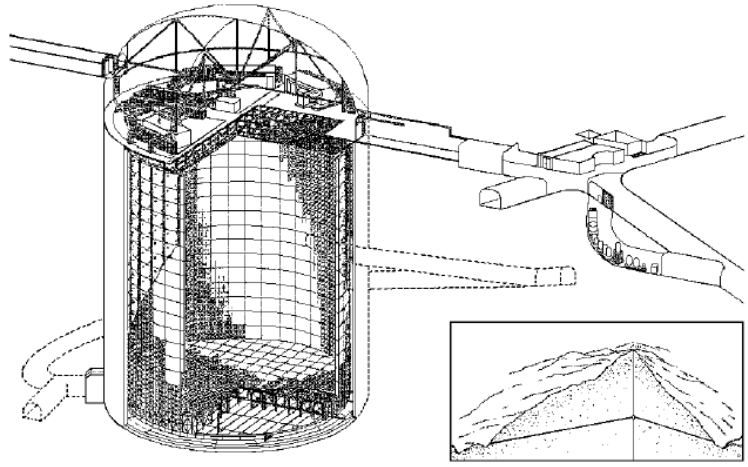

Figure 3: View of Super-K tank and Kamioka mine

Super-K consists of an outer detector and an inner detector. Inner detector has 32000 tons volume and 11129 20-inch photon-multiplier tubes (PMT) with about 40% coverage, while outer detector has 1885 8-inch PMTs [11]. PMTs are installed in the top, barrel and bottom of the tank by stainless frames. Rate of muon events in Super-K is about 1∼2Hz, outer detector is used to recognize the muon events. For such purpose, the wall of outer detector is covered with white tyvek sheets of about 80% reflection to increase the photon collection efficiency. And oppositely, to decrease the reflection and the possibility of mis-reconstruction, inner detector is covered with black sheets.

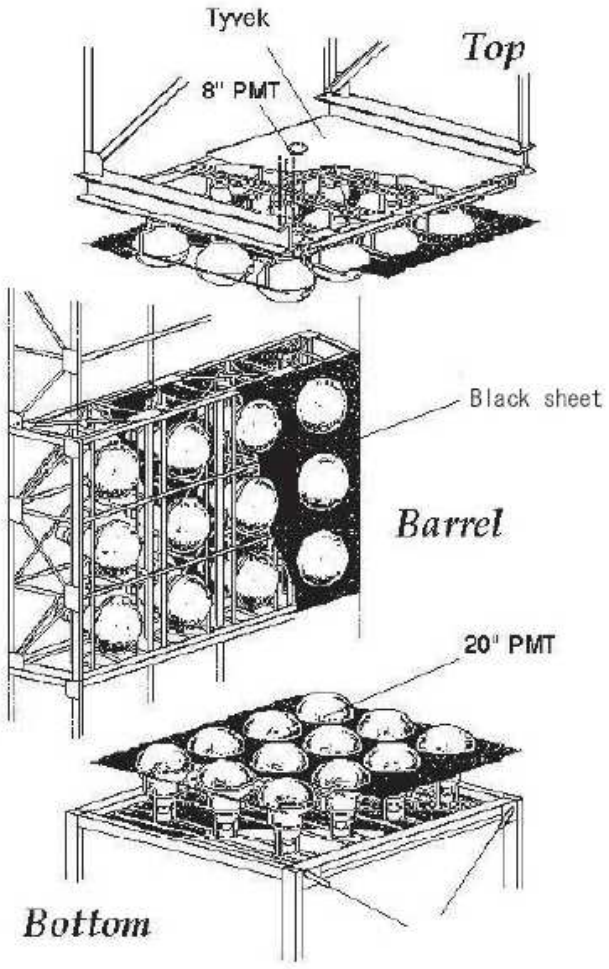

Figure 4: Stainless frame of top, bottom and barrel PMTs. The surface of the PMTs are covered with black sheet to reduce reflection.

The construction work of Super-K began in 1991 and be finished in 1996. The purpose of the Super-K is various neutrinos physics and the measurement of proton life time. It observed solar neutrinos [12], atmospheric neutrinos [13] as well as accelerator neutrinos [14], and several evidences for neutrino oscillations were found. Super-K detector started to take data from April 1996 and now it is running as fourth phase. Super-K has been collecting data for nearly twenty years and it is still the largest neutrino detector in the world.

2.2 Cherenkov radiation

The speed of light in medium is c/n, when the index of refraction is n. If a charged particle passes through the medium with velocity larger than c/n, the particle will emit a forward cone of light. This is named as Cherenkov radiation, while P.A.Cherenkov is the person who discovered this effect in 1934. To theoretically explain it, when a charged particle travels in the medium, it

Particle	Threshold(MeV)
$e^{\pm}$	0.767
$\mu^{\pm}$	157.4
$\pi^{\pm}$	207.9

Table 1: Cherenkov threshold for charged particles in water.

will emit spherical wave by electric polarization. If the velocity of the particle exceeds c/n, the spherical waves can interfere with each other and form radiation (Figure 6). Otherwise, they will never meet each other and stay independent (Figure 5).

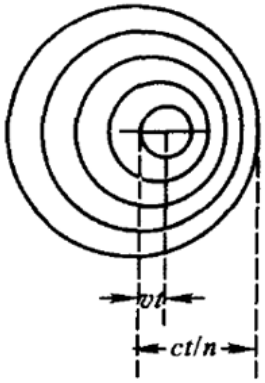

Figure 5: when velocity of the charged particle is smaller than c/n

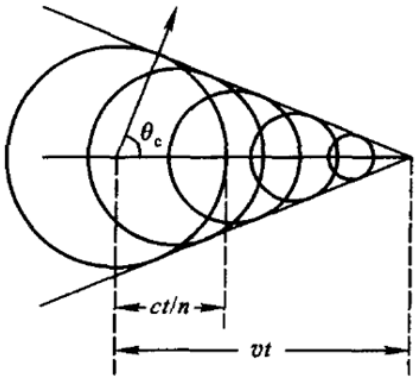

Figure 6: when velocity of the charged particle is larger than c/n

Thus, the angle between Cherenkov light and the direction of the charged particle can be calculated with the ratio of light velocity in the medium c/n and the velocity of incident particle as follows:

$$\cos\theta = \frac{1}{n\beta} \tag{9}$$

Here $\beta = v/c$. Considering the critical condition of Cherenkov radiation is $\beta \geqslant 1/n$,the energy threshold for incident particle to emit Cherenkov light is:

$$E_{thr} = \frac{nm}{\sqrt{n^2-1}} \tag{10}$$

For water Cherenkov detector, the index of refraction is 1.33, so the threshold of total energy for the main particles is shown below.

In most cases, the signals observed in Super-K are from electrons or muons with $\beta \approx 1$, so the Cherenkov angle is close to 42°. The number of photon (N) produced by Cherenkov radiation in unit length dL can be calculated as:

$$\frac{d^2N}{d\lambda \mathrm{d}L} = \frac{2\pi\alpha Z^2}{\lambda^2}(1 - \frac{1}{n^2\beta^2}) \tag{11}$$

Here λ is the wavelength of Cerenkov radiation, Z is the charge of incident particle, and α is fine-structure constant. By integrating it, the number of photon in specific wavelength range (λ_1, λ_2) is:

$$\frac{dN}{dL} = \frac{2\pi\alpha Z^2}{n}(\frac{1}{\lambda_1} - \frac{1}{\lambda_2})(1 - \frac{1}{n^2\beta^2}) \tag{12}$$

For example, when an electron travels 1cm in Super-K tank with $\beta \approx 1$, about 340 photons would be produced in Super-K PMT sensitive range of 280nm∼660nm. It can hardly be observed and that is why we need photon-multiplier tubes (PMT).

2.3 Neutrino interaction in water Cerenkov detector

Supernova emits neutrinos and anti-neutrinos in three flavors. These neutrinos react with water and finally charged particles are observed by Cerenkov radiation. The main reactions of neutrinos in water Cerenkov detector is shown below.

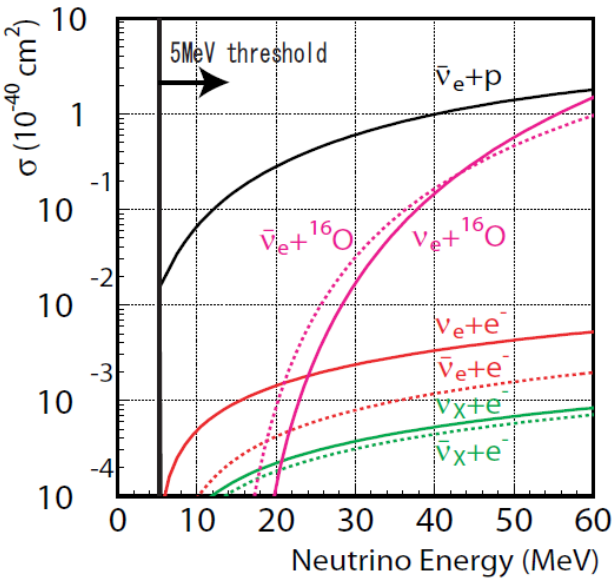

Figure 7: Cross section comparison of various neutrino interaction in 0∼60MeV range [15]

Inverse Beta Decay:

$$\overline{\nu}_e + p \rightarrow n + e^+ \tag{13}$$

This is the most dominant interaction and it has the largest cross section in the energy region of Supernova neutrinos. It occurs between the anti-neutrinos of electron type and the free protons in the water. Most of supernova neutrinos will be detected via this interaction. However, the direction information will be lost in this interaction.

Photoelectronic Surface	50cm
Material	Sb-K-Cs
Dynode	Venetian Blind type
Quantum Efficiency	22% at 390nm
Dark Rate	3.5kHz
Time Resolution	3ns RMS at 1pe

Table 2: Properties of Super-K inner PMT

Neutral Current Interaction:

$$\nu_x + {}^{16}O \rightarrow \nu_x + \gamma + X \tag{14}$$

Elastic Scattering:

$$\nu + e^- \rightarrow \nu + e^- \tag{15}$$

This is the elastic scattering between neutrinos and electrons in water. It happens in all flavours, but the electron-neutrino has about 6 times larger cross section than others because of charged current interaction. The cross section is two order smaller than inverse beta decay but it can conserve the direction information of the incident neutrinos, which is very important for the early announcement to the other measurement such as optical observation, gamma-ray and so on.

2.4 Photomultiplier tube

The PMTs being used in Super-K are produced by Hamamatsu Photonics c.o, and the development work was done under the cooperation of Super-K group. The inner detector PMTs are 20-inch Hamamatsu R3600 PMTs, and the outer detector PMTs are 8-inch Hamamatsu R1408 PMTs. The design of inner detector PMTs are based on the PMTs being used in KamiokaNDE experiment, with several improvements.

Figure 9 shows the structure of a PMT. The photo-cathode is made of bailkali (Sb-K-Cs) and it is sensitive to photons with wavelength in 300∼600 nm, which covers the wavelength of Cherenkov light. Electron photons could be multiplied with a gain of $\sim 10^{\ 7}$ by 11 chain dynodes. Super-K PMTs not only have better time resolution than Kamiokannde PMTs, but also become able to identify single photon signals. It is an improvement of great significance because most of the signals in low energy events like supernova neutrinos are due to single photon.

Figure 8: Photo of a bare PMT

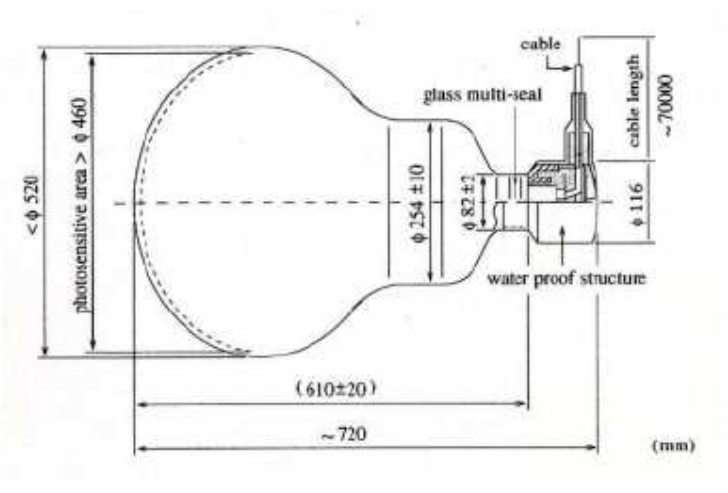

Figure 9: Inner structure of PMT

Figure 10: The acrylic cover and FRP case used from 2001 to protect the PMT from shock wave

The threshold is set to 1/4 pe and the rate of dark noise above this threshold was ∼3.5 kHz when in Super-K first phase. The magnetic field of the earth can largely affect the photoelectrons so Helmholtz coils are used for compensation. The residual geo-magnetic field is kept less than 100 mG in every position of the tank.

In the accident happened in 2001, about half of the PMTs were broken as a result of shock wave. Since that, PMTs in Super-K are all installed with acrylic covers and FRP cases as shown in Figure 10. The transmittance of the acrylic cover is about 96% and it doesn't affect the event reconstruction.

2.5 SRN detection in Super-Kamiokande

The reason why SRN has not been observed is high background and low event rate. As the largest water Cherenkov detector in the world, Super-K has the largest volume and the best sensitivity for SRN flux. The event rate of SRN between 10MeV and 30MeV is expected to be about 1.3-6.7 events/year/22.5kton in Super-K.

In SRN detection, inverse beta decay plays an important role, because its cross section is two orders of magnitude larger than ν_e elastic scattering with electron, which is the second most visible interaction of SRN in Super-K. Currently, IBD only has a Cherenkov signal emitted by positron. The neutron produced in IBD will be thermalized in water and then be captured by free protons, with a result of 2.2 MeV gamma ray emission. The coincidence detection of positron and neutron can effectively reduce the background. Neutron tagging will also enable Super-K to identify electron-neutrinos and anti-electron-neutrinos, which is very important for the investigation of supernova explosion mechanism and will also largely improve the precision of other neutrino physics.

However it is very difficult to detect 2.2MeV gamma rays as it is below the detection threshold and thus the method of tagging neutrons by 2.2MeV gamma ray has a very low efficiency. Because of these, adding gadolinium into Super-K was proposed [16]. The cross section of thermal neutron capture on natural

gadolinium is 49000 barn, while 0.3 barn on free protons. And neutron capture on ^{155}Gd and ^{157}Gd can emit 8.5MeV and 7.9MeV gamma rays respectively. It will make neutron tagging much easier and more efficient than 2.2MeV gamma.

$$n + Gd \rightarrow Gd + \gamma's(8MeV) \tag{16}$$

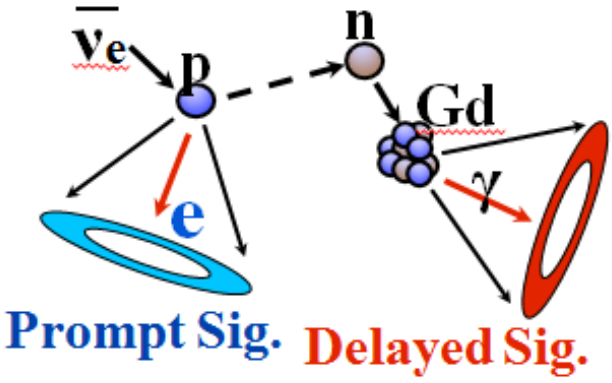

Figure 11: Detection principle of using gadolinium to produce delayed signal

By this way, inverse beta decay will have two signals, positron signal is the prompt one and the ∼8 MeV gamma cascade from neutron capture on gadolinium is the delayed one. Background for SRN can be largely reduced by detecting prompt and delayed signals coincidently, and Super-K will also have the ability to distinguish neutrino and anti-neutrino. As will be discussed later, now a lot of R&D works are ongoing and the project of adding gadolinium into SK is called SK-Gd project.

3 SK-Gd project and EGADS

3.1 EGADS Detector overview

3.1.1 200 tons water tank

It is essential to understand what will happen after loading gadolinium water and estimate all the potential effect. The most direct and efficient way is to build a similar detector with the same conditions as Super-K. Such R&D project is called Evaluating Gadoliniums Action on Detector System (EGADS), which was funded in 2009 and proposed to test gadolinium effect on Super-K. In gadolinium loaded detector, most of the neutrons produced by inverse beta decay will be captured in 2m distance. Thus, the size of EGADS detector does not need to be so large. Finally the tank was designed as a 200m^3 stainless steel tank and built inside Kamioka mine in 2010, several tens of meters from SK tank. 240 20-inch PMTs were installed into EGADS tank and its own data acquisition system has been developed. Within these 240 PMTs, 224 of them are the same with Super-K and 16 of them are prototypes which will be tested for Hyper-K. And also, 18 of the 224 Super-K PMTs are installed with FRP cases and 60 are installed with both FRP cases and acrylic vessels, while the remaining 146 are bare ones. Gadolinium sulfate ($Gd_2(SO_4)_3$) was chosen for our candidate as will be discussed later. The work of filling gadolinium into EGADS tank started from November 2014. The filling work was finished by April 2015 and 0.2% gadolinium sulfate has been dissolved. A 90% efficiency of neutron capture is expected under this concentration.

Figure 12: Photo of EGADS underground lab inside Kamioka mine

3.1.2 Water system

To dissolve gadolinium into Super-K, an important thing is the upgrade of the current water system. The major importance is the stability of water

quality, so the system should have the ability to remove the impurities and keep the water quality at a good level. What's more, gadolinium should be gathered and reloaded into the tank after purification when the water is passing through the system. A prototype of the circulation system for gadolinium loaded water was developed at University of California, Irvine (UCI) long before EGADS project started and now the system has already running for more than one year. Gadolinium loaded water pumped out from EGADS tank will first go through an ultra-filter, which removes the impurities larger than gadolinium. Then the water will be filtered by two nano-filters, which filter out the particles of about the same size of gadolinium, and the gadolinium concentrated water rejected by the filters will be lead to a buffer tank. Then the water passed from the nano-filters will go through reverse osmosis membranes(RO) to remove smaller impurities. Water is also treated with deionizers, UV lights and micro-filters to ensure that anions of about the same size of gadolinium or organic carbons are removed. Finally the purified water will go into the collection buffer tank and be mixed with the gadolinium concentrated water and then be injected into EGADS tank again.

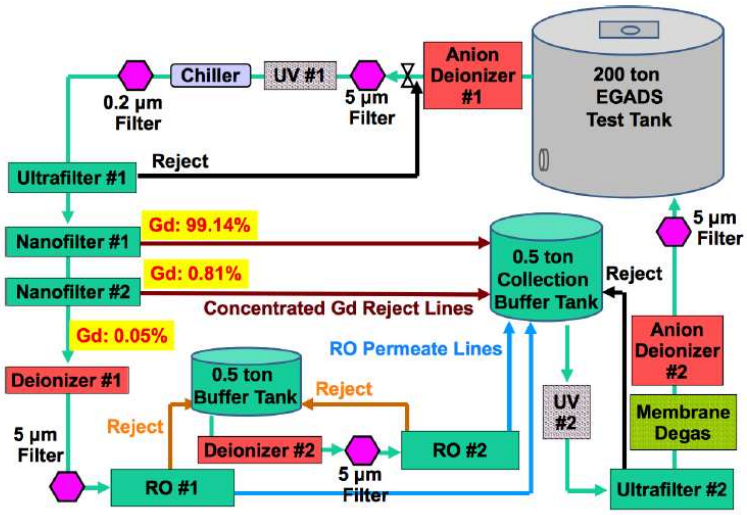

Figure 13: Structure of water circulation system of EGADS

A pre-mix 15 ton tank has also been installed together with a pre-treatment system. Gadolinium sulfate will be mixed in this 15 ton tank before being injected into EGADS tank. The pre-treatment system has a stirrer to facilitate the dissolution of gadolinium sulfate in water.

3.1.3 Electronics and Trigger

The signals from the PMTs are sent to front end modules called Analog Timing Module(ATM). One ATM board can treat the signals from 12 PMTs and 20 ATM modules are being used. If the input signal into the ATM exceeds the threshold level, ATM will produce a 200 ns width and -15 mV height signal called HITSUM. HITSUM generated from the front panels for all the ATM modules are summed up and sent to a discriminator, which determines the

trigger threshold of DAQ system. For example, the threshold of prompt trigger in normal run mode is -110mV, this is equal to about 45 PMT hits, which means signals are outputted from 45 PMTs within 200ns. In ATM module, both signal timing and integrated charge are digitalized. Such information is recorded and transferred to a front-end Linux PC, as well as the trigger timing and trigger type of each event.

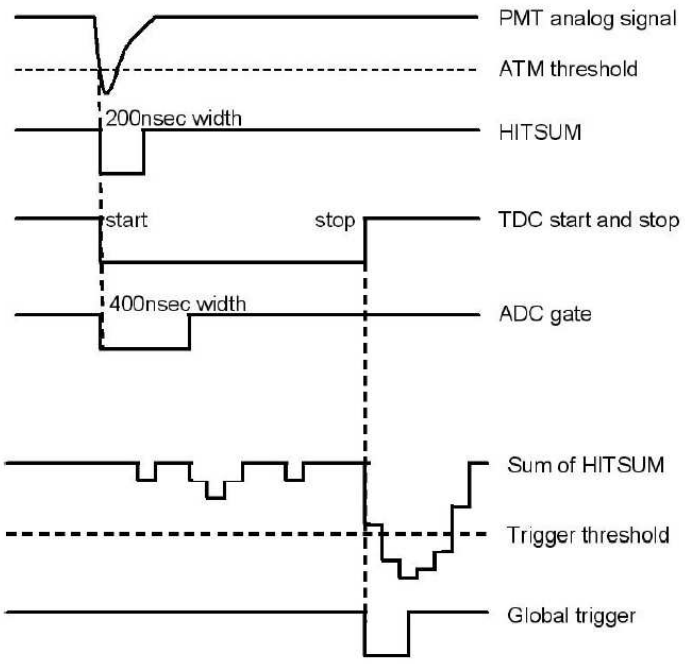

Figure 14: Trigger system and HITSUM signal

Raw data in binary format is saved in the front end PC in the mine. A program called real time process is checking the data and DAQ status. Every 8 hours, the real time process will sent the raw data to the online computers in computer building outside the mine. The raw data will be converted into analysable format by online computers, and can be used in offline analysis later.

3.1.4 Gadolinium concentration

We are doing our best to make the gadolinium concentration to be uniform in the tank and we expect the concentration to be as stable as possible. But actually the gadolinium concentration is slightly different in different position and changes with time. So it becomes necessary to monitor how uniformly we could dissolve gadolinium as well as to check how well the water system works. For such purpose, UDEAL is used to take samples from top, centre and bottom of the tank. The samples are measured with an atomic absorption spectrometer(AAS) with an measurement uncertainty of 3.5%.

Figure 15: Photo of the Zeeman atomic absorption spectrometer in EGADS lab

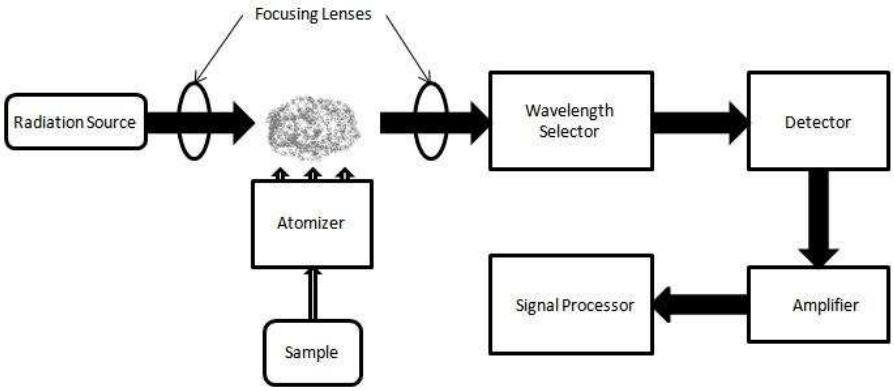

Figure 16: Scheme of the Zeeman AAS machine

The scheme of the Zeeman AAS machine used for this measurement is shown in Figure 16. Since 0.2% gadolinium concentration is too high for the cuvette of Zeeman AAS machine, the samples are diluted and compared with standard solutions. Standard solutions are used for calibration of the machine every time when it is switched on. The diluted sample is heated and atomized and then be shined by the light from hollow cathode lamp. The light amount absorbed by the sample is proportional to the gadolinium contained in the sample.

3.2 Water transparency

3.2.1 Soak test

Adding gadolinium may influence the material aging. We need to ensure that adding a gadolinium solution will not corrode or easily age detector materials.

The materials used for the construction of EGADS and Super-K tank are tested in Okayama University. The samples of these materials are soaked in gadolinium water in 500ml or 250ml bottles and be kept in thermostats chambers at 15°. They are tested under different conditions such as gadolinium concentration and temperatures.

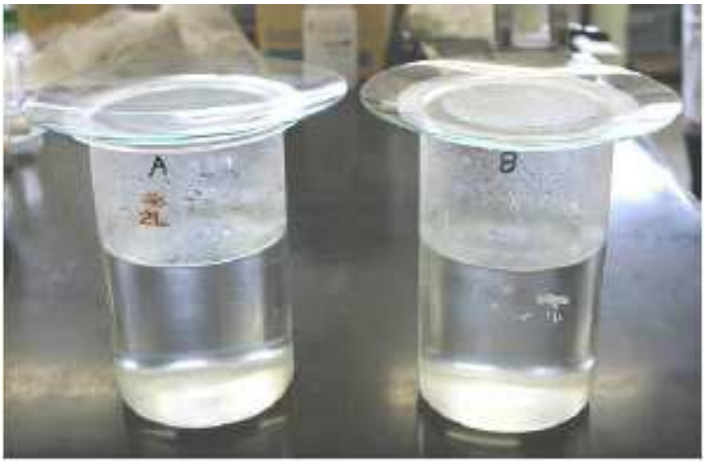

Figure 17: Sample of pure water and gadolinium dissolved water

The transparency of the water soaked with samples can be measured with spectrometer. The wavelength range of the spectrometer are set as 200nm∼800nm, while the sensitive range of PMT is about 280nm∼630nm. The transparency comparison of pure water and 0.2% gadolinium water without any samples are shown below. Though the transparency decreases below 250nm, it doesn't affect our detection because it is out of PMT sensitive range. $GdCl_3$ was proposed in the past. However, a test with one kiloton water tank with 0.2% of $GdCl_3$ showed that although $GdCl_3$ did not decrease water transparency, chlorine lifted old rust already present in the one kiloton tank and it has been confirmed by soak test. Now our new candidate is $(Gd_2(SO_4)_3)$. After we loaded gadolinium sulfate, rust was once found in the tank. After soak test we found out that the rust was due to a kind of wire used to fix blacksheet in EGADS tank. It is a newly used material and it is not being used in Super-K. Other materials such as mine guard which is our candidate for leak fixing in the future, are also carefully tested with promising results.

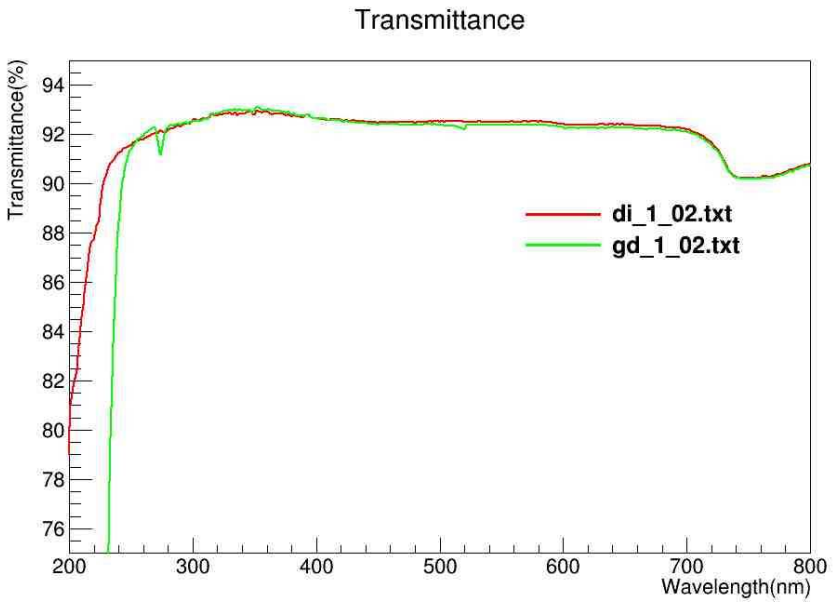

Figure 18: Transmittance comparison of pure water and gadolinium water. Red line is distilled water and green line is gadolinium water.

3.2.2 UDEAL system

In order to monitor the water transparency change in the tank, a measurement device called Underground Device Evaluating Attenuation Length (UDEAL) was developed at UCI. This device consists of a beam injector, a intensity monitor (upper part), pipe (middle) and transmitted light instrument (below the pipe).

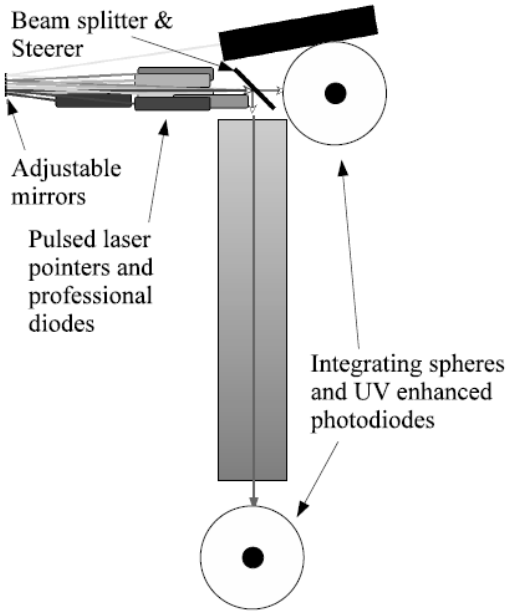

Figure 19: Scheme of UDEAL device

UDEAL can take water samples automatically from three positions (top, centre, bottom) of the tank, and measure the samples with laser by seven different wavelengths (337nm, 375nm, 405nm, 445nm, 473nm, 532nm and 595nm). These wavelengths cover the main range of Cherenkov light signals in Super-K. By using the measurement results of UDEAL, water transparency is evaluated as the intensity of Cherenkov light left at a distance of 15 m (LL_{15m}). Time-related change of water transparency is shown in Figure 20. Gadolinium sulfate was injected into the tank by four times, after the injection transparency got down suddenly, and then recovered as a result of circulation. Measurement with spectrophotometer and other studies are also being performed.

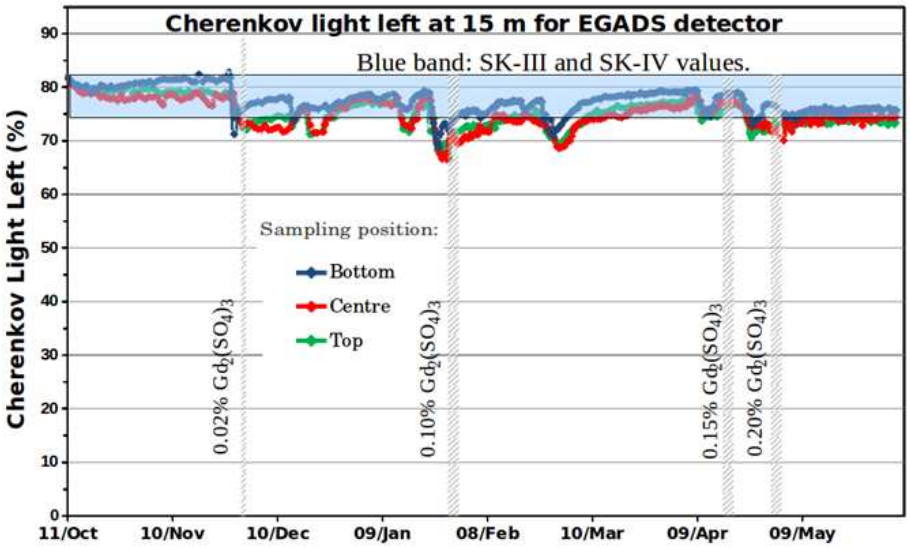

Figure 20: Water transparency change measured by UDEAL. It is estimated by LL_{15m}.

3.3 Detector calibration

3.3.1 HV setting

In PMT calibration, Quantum Efficiency (QE) and gain are two important factors. Here, QE also includes the collection efficiency of photoelectrons onto the first dynode of the PMT. Gain is the conversion factor from the number of collected photoelectrons to output charge (in units of pC). Low energy events like SRN signals usually consist of single photoelectron (pe) hits so their analysis heavily depends on QE calibration, while high energy events depend more on gain calibration. The output of the PMT depends on the voltage applied on it. So first of all, we need to determine the high voltage value for all the PMTs. PMTs with the same geometry are divided into one group and the target of high voltage calibration is to make the PMTs in the same group to have a same output value.

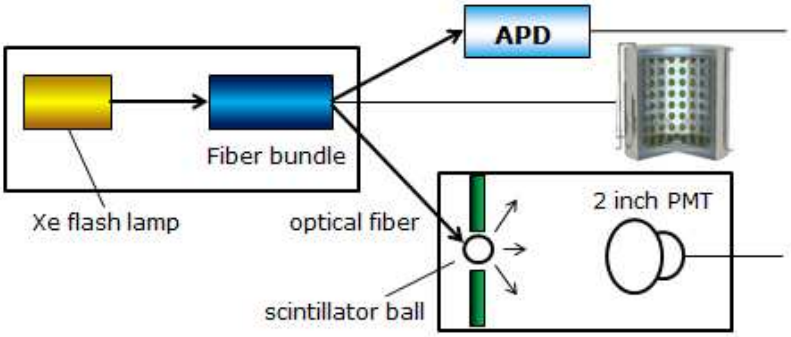

Figure 21: Setup of the measurement of Xe scintillation light

For this calibration, we use Xe flash lamp as a light source. Light from the lamp passes through a UV filter and then be injected into the tank through optical fiber, finally arrive at a scintillator ball placed in the center of the tank. The other two fibers go to an avalanche photodiode(APD) module and a dark box installed with a 2 inch PMT, which are both used to monitor the light intensity of Xe lamp. The scintillator ball is an acrylic ball containing 15ppm POPOP as a wavelength shifter and 2000ppm MgO as a diffuser to make the light emission from the ball as uniform as possible.
After high voltage adjustment, a table of high-voltage setting for each PMT was made and this table has been loaded into electronics system. Figure 22 shows that the difference between every PMT and the average value of its group is less than 1%, with 0.003% RMS.

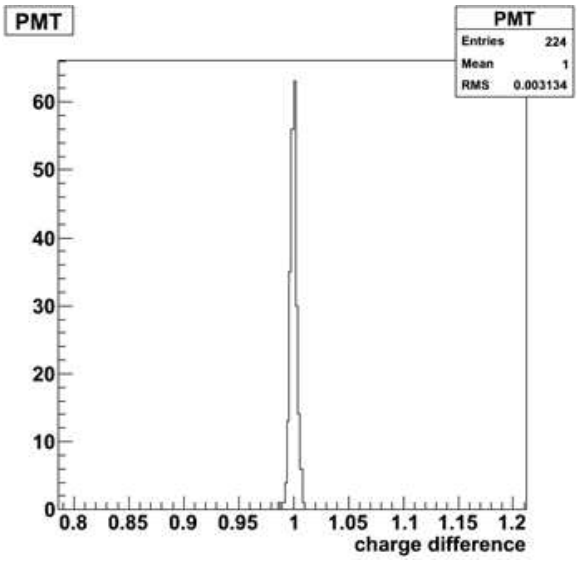

Figure 22: Distribution of charge difference of normal PMTs after HV adjustment

3.3.2 Timing correction

Timing for each PMT has to be calibrated for precise reconstruction of event vertices. However, the transmit time, cable length and processing time of read-out electronics of each PMT are different, as a result the time response of each PMT also varies. Besides, we have to consider a so-called timing-walk effect, it means the timing of discriminator output is related to the pulse height of PMT signal. As shown in Figure 23, the rise time of a large pulse is faster than that of a smaller one.

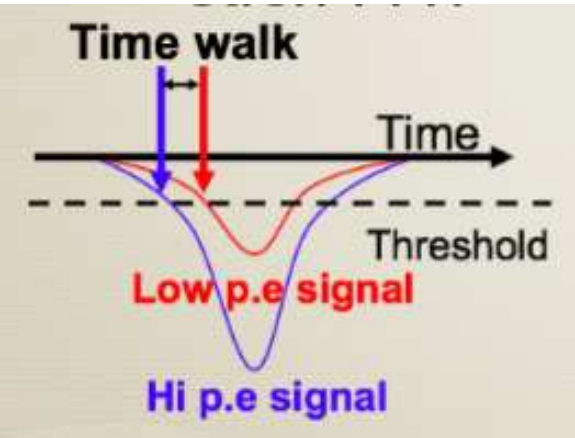

Figure 23: Time walk effect

Including all these above, we propose to make a charge-timing correction for each PMT to make relative timing difference as small as possible, such correction constants is called TQmap. Every PMT has its own TQmap because the character of each PMT is unique. Figure 24 shows an example of TQmap of one PMT. As discussed before, higher charge hits have earlier timing and better resolution.

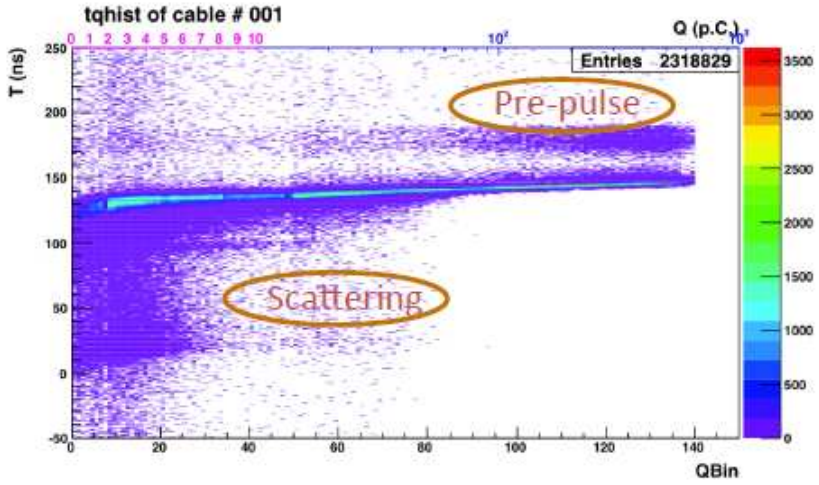

Figure 24: TQ distribution of the PMT with ID 1

To calibrate PMT timing, we use a nitrogen laser as a light source. The nitrogen laser(USHOKEC-100) can emit light of 0.4ns FWHM at a wavelength of 337nm. A dye is used to shift the 337nm light to 398nm, where the light absorption spectrum and quantum efficiency of the PMTs are almost maximum. The laser output is monitored by a fast response 2 inch PMT, which is also used to produce timing trigger for DAQ system. The output light from laser is leaded into the tank by optical fiber and then be emitted from a diffuser ball placed in the centre of the tank. Directional variations in the photon emission time of the diffuser ball were measured to be less than 0.2ns.

3.3.3 Quantum efficiency measurement

The absolute value of quantum efficiency (Q.E.) of PMTs is measured by Hamamatsu Photonics when these PMTs were produced. QE depends on the wavelength of photons, and their relationship is shown in Fig 25. As can be seen from this figure, the value of Q.E. at the typical wave length of Cherenkov light ($\lambda = 390$nm) is 22%.

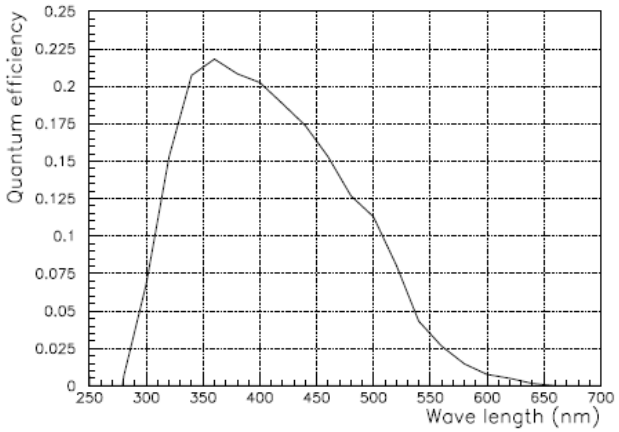

Figure 25: Absolute Q.E. values of PMT depending on wavelength

Figure 26: Ni ball used for relative Q.E. measurement [17]

However, the conditions of every PMT are not completely the same so that the relative QE slightly differs from each other. The Relative QE of each PMT is measured by Ni-Cf source. This source is made by ^{58}Ni ball and a ^{252}Cf stick is inserted into the ball. Neutrons are provided by ^{252}Cf, and 9MeV gamma rays are emitted isotropically by neutron capture on ^{58}Ni. More than 99% of observed signals are due to single pe. The source is made like a ball as shown in the Figure 26. When measuring QE of PMTs, Ni-Cf source was placed at the centre of the tank, and relative QE can be calculated by counting rate of each PMT. Of course, the distances from the source to PMTs in different positions are different so the PMTs will detect different numbers of photons. To take the position effect into consideration, MC simulation is used and the experiment data is compared to MC results to cancel the geometry differences. The dispersion of relative QE was measured to be 5.7% of RMS.

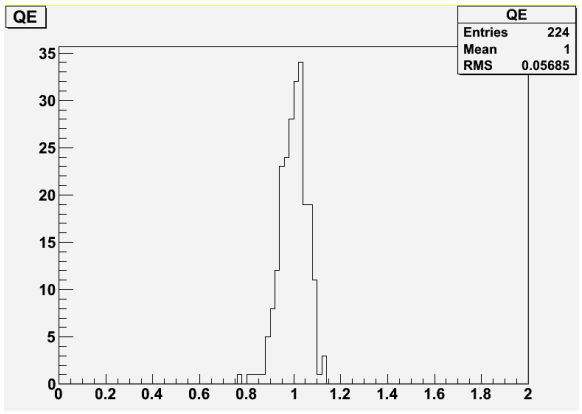

Figure 27: Relative Q.E. difference

3.3.4 Gain measurement

Similarly to QE measurement, we need to measure the absolute and relative value of PMT gains. As gain means the proportion of photoelectron numbers and PMT output charge, absolute gain can be calculated from the charge distribution of single photon signals. LED was chosen to be the light source. LED light is injected into the tank by optical fiber and finally emit from the diffuse ball which is also used for timing calibration. Diffuser ball was placed in the centre of the tank and the light output of LED was carefully controlled to ensure the light arrived PMT surface is at single photon level. The charge distribution of single photon signals is shown in Figure 28 as green line.

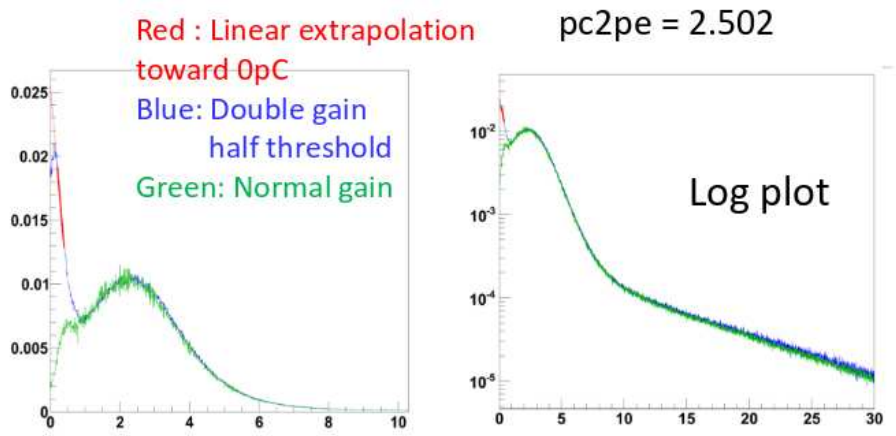

Figure 28: Charge distribution for one pe signals. Left is linear scale and right is the same figure in log scale.

The green line in the Figure decreases in low charge parts, it is due to the threshold of ATM modules used in electronics. To extend this distribution to low charge parts, we reduced the ATM threshold to half of normal values, and raise the PMTs gain to double of normal values by high voltage setting. The result is shown as blue line in the Figure. The distribution is better than the green one but it still decreases in very low parts because the ATM threshold is not completely zero. However, the single photon distribution could be considered to be linear below 0.5pC so we can extend this distribution to zero by fitting it using linear function. The result is shown as red line and we integrated it to obtain the conversion factor from observed charge to photo-electron value. The latest result is 2.502 from pC to pe.

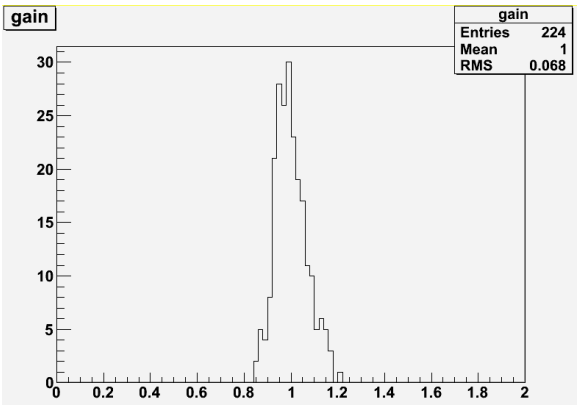

Figure 29: Relative gain difference

For relative gain, it is measured with laser diode. Here, we need two measurements using the same light source to reduce the geometrical effect. In the first one we emit high intensity flashed from the centre of the tank to make each PMT can get a suitable number of photons, and then calculate the average charge of each PMT. In the second measurement, we emit low intensity flashed to make sure that every event only hit a few PMTs so that almost all of these signals are single pe. By taking the ratio of the average charge in the first measurement and the hit rate in the second measurement, relative gain of each PMT can be estimated. Figure 29 shows the relative gain distribution for each PMT, and its dispersion was measured to be 6.8% of RMS.

All of these calibration works were carried out when EGADS tank was filled with pure water. And other works such as Rayleigh scattering measurement were also performed.

3.3.5 Long term stability

After basic calibration works described in the previous sections, it is also important to monitor the long term performance of the PMTs. So we installed the Xe flash lamp with scintillator ball into a side hole of the tank as a long term monitor. The side hole is about 2m from the centre hole. The time-related change of PMTs is termly checked.

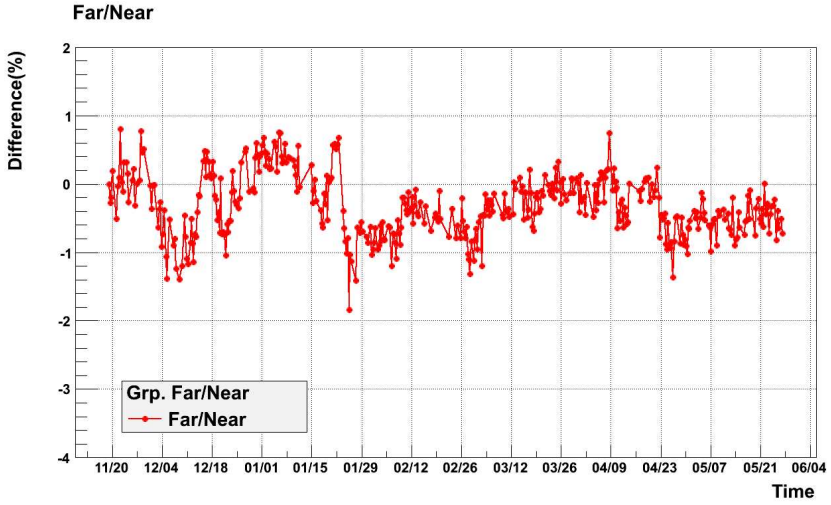

Figure 30: Water transparency change monitored by Xe trigger. It is estimated by the ratio of the output charge of the most distant PMTs and the nearest PMTs.

This monitor can also be used to make a cross check for the water quality change in the tank. We choose the farest and nearest PMTs from the scintillator ball and take the ratio of their charges. The long term change of the ratio is shown in Figure 30, it has the same trend with the water transparency measurement of UDEALtransparency decreased suddenly when gadolinium sulfate was injected, and then recovered after circulation system started running.

4 EGADS data analysis

4.1 Event reconstruction

The vertex of event is the position where the electron or muon exceeds Cherenkov threshold and begin to produce Cherenkov light. By strict saying, it is not a point but a track because the charged particle will continue to emit Cherenkov light as long as its velocity is larger than light. However, in case of low energy events like SRN, the scattered electrons can only go through several cm in water, while the vertex resolution in Super-K is about 100cm. Thus, the track length is negligible and the vertex can be regarded as a point. In addition, the number of photons produced in low energy events is so little that most of the PMTs can only get a single photon signal. This means, reconstruction of low energy events only need the timing information, while high energy events also need to use charge information of the PMTs. Super-K has several software tools for the reconstruction of low energy events. The latest one is called Branch Optimization Navigating Succesive Annealing Iterations (BONSAI). It is developed on the base of Kai-fit, Clus-fit and Hayai, which were used in the past. BONSAI has the best precision and resolution but it cost more time for calculation than the others [18]. BONSAI fitter has been replanted to EGADS, with the detector size and PMT position redefined. Other modifications are also applied according to the conditions of EGADS.

4.1.1 Vertex reconstruction

The first thing of event reconstruction is to determine the vertex of the event by using the timing signal and the positions of the PMTs. The real time when the charged particle begin to produce Cherenkov light is obtained by subtracting time of flight (TOF) from output timing information of each PMTs.

$$t_{res,t} = t_i - \frac{n}{c}\sqrt{(x-x_i)^2 + (y-y_i)^2 + (z-z_i)^2} \tag{17}$$

Here i means PMT number, n/c means velocity of light in water, t_i and (x_i, y_i, z_i) are the position and timing signal of the PMTs. In ideal case we expect the reconstruction position to make $t_{res,i}$ of all the hit PMTs to be equal. However there always exist background hits, which are caused by after-pulse, dark noise, reflection or else. To take them into consideration, BONSAI calculates the likelihood of every event as:

$$L(\vec{x}, t_0) = \sum_{i=1}^{N_{hits}} \log(P(\Delta t_i(\vec{x}))) \tag{18}$$

Here t_0 is the average time of selected hits, and t_i is the result of subtracting t_0 from each $t_{res,t}$. $P(\Delta t_i(\vec{x}))$ is the possibility density function of typical Cherenkov events. In Super-K, there is a calibration device called LINAC, it can accelerate electrons and introduce them into the tank. The PDF used for event reconstruction in Super-K is evaluated by LINAC, but EGADS doesn't have such device so the PDF of EGADS is made by Monte Carlo simulation. After-pulse, dark noise and other parameters are well tuned by Cf-Ni source to make sure MC and data have good agreement. Details are shown in 4.1.1.

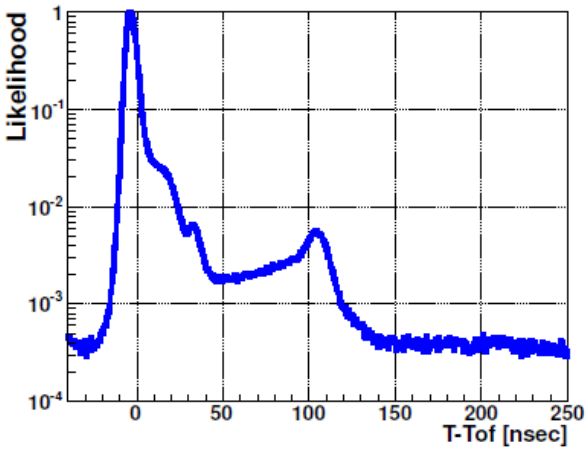

Figure 31: The likelihood function which BONSAI uses for vertex reconstruction. The peaks around 40ns and 100ns are due to after pulse. [19]

BONSAI will search the best vertex by maximizing the likelihood. The fitting precision can also be estimated by the value named "goodness". It is defined as:

$$goodness = \frac{1}{\sum_{i=1}^{N_{hits}} \frac{1}{\sigma^2}} \times \sum_{i=1}^{N_{hits}} \frac{1}{\sigma^2} exp(-\frac{{t_{res,t} - t_{mean}}^2}{2\sigma^2}) \tag{19}$$

σ is the time resolution of the PMTs. Goodness ranges from 0 to 1, while an ideal event will have a value of 1.

4.1.2 Direction reconstruction

After determining the vertex of the event, we should determine the incident direction. Since the mass of electron is so little that in most of the cases the scattered electron has a velocity of $\beta \approx 1$, even in low energy events like supernova neutrinos. Therefore, Cherenkov angle of the signal is expected to be close to 42 degrees. However, the real signal does not perform to be a clear ring shape because of several effects like the multiple scattering of electron in water, the scattering and reflection of Cherenkov light, dark hits and so on. To determine the direction with a better precision, firstly the $t_{res,i}$ of all the hit PMTs are calculated and only the ones which are in the 50ns time window around the peak are selected. The maximum number of hit PMTs in this 50ns window is called N_{50}. The direction is determined by the selected PMTs by maximizing the likelihood as [20]

$$L(\vec{d}) = \sum_{i=1}^{N_{50}} log(P_i(cos\theta_{dir})) \times \frac{cos\theta_i}{a(\theta_i)} \tag{20}$$

The function $P_i(cos\theta_{dir})$ is the possibility density function of the opening angle between the incident direction and the vector from vertex point to hit PMT. The PDF is made by Monte Carlo simulation. θ_i is the incident angle of Cherenkov

light to PMT surface, and the function $a(\theta_i)$ describes the acceptance of the photon by the photo-cathode of the PMT. The initial direction is calculated as the sum of the vectors from the vertex point to all the PMTs selected by N_{50}. Then the direction will searched with a spacing of 20 degrees, 9 degrees, 4 degrees and finally 1.6 degrees. In Super-K the direction resolution of 10MeV electron is about 27 degrees according to LINAC calibration, so this search spacing is small enough.

$$\vec{d}_{init} = \sum_{i=1}^{N_{50}} \vec{v}_i \tag{21}$$

4.1.3 Energy reconstruction

Roughly, the energy of incident particle is in proportion to the number of photons produced by Cherenkov light. For low energy events, the number of photon is very little, for example, a 16MeV electron can only produce 2600 photons. In such events, PMTs could only get signals of one photon. So the energy of incident particle can be calculated only by the number of hit PMTs, instead of using their output charge. Another advantage of this method is, the calculation will not be affected by PMT gain. The charge distribution of one photon signal is shown in previous chapter. It is very difficult to recognize the number of photoelectrons when the signal is at a level of only several photons. Because of all these above, N_{50} is used for energy reconstruction, and corrections are applied to obtain the effective hits.

$$N_{eff} = \sum_{i=1}^{N_{50}} [(X_i + \epsilon_{tail} - \epsilon_{dark}) \times \frac{N_{all}}{N_{alive}} \times \frac{R_{cover}}{S(\theta_i, \psi_i)} \times exp(\frac{r_i}{\lambda}) \times G(i)] \tag{22}$$

X_i : correction for multi-photonelectron
When the event occurs near the wall of the tank, and the Cherenkov light goes forward to the wall, then the number of hit PMTs will be very little and each PMT will have high possibility to get more than one photon. This effect is corrected by taking the ratio x_i of hit PMTs in the 3×3 area surrounding the i-th PMT and the total number of hit PMTs. X_i is defined as:

$$\begin{cases} (log\frac{1}{x_i - 1})/x_i & x_i < 1 \\ 3.0 & x_i = 1 \end{cases} \tag{23}$$

In this correction, it is assumed that the photons are uniform in the 3×3 area and their distribution follows Poisson statistics.

ε_{dark} : correction for dark noise

$$\varepsilon_{dark} = \frac{50ns \times N_{alive} \times R_{dark}}{N_{50}} \tag{24}$$

Dark hits may occur in the 50ns window accidently so it should be subtracted from the effective hits. N_{alive} is the number alive PMTs and R_{dark} is the rate of dark hits. In EGADS, dark rate is monitored by Laser Diode every day.

ε_{tail} **: correction for reflection**
If Cherenkov light is reflected, it will acts as a late hit outside the 50ns window. This is corrected as:

$$\varepsilon_{tail} = \frac{N_{100} - N_{50} - N_{alive} \times R_{dark} \times 50ns}{N_{50}} \tag{25}$$

Similarly to the definition of N_{50}, N_{100} is the maximum number of hit PMTs in 100ns time window.

$\frac{N_{all}}{N_{alive}}$ **: correction for dead PMTs**
A correction for PMTs which are not working well.

$\frac{1}{S(\theta_i,\psi_i)}$ **: correction for the coverage of photo-cathode**
The effective coverage of photo-cathode depends on the incident angle of photons. Details about it can be found in reference.

$exp(\frac{r_i}{\lambda})$ **: correction for water transparency**
This is a correction for the photons lost by the reason of scattering or absorption in the water. Here r_i is the distance from vertex to i-th PMT, and λ is the measured transparency.

G_i **: correction for gain difference**
It is a correction for the relative gain difference of the PMTs.

As discussed before, the energy of charged particle is roughly in linear proportion to the effective hit number. In Super-K the function to scale the energy is calibrated by LINAC, while in EGADS we use MC simulation. Electrons with energy of 2∼15MeV are generated in simulation and the relationship between N_{eff} and energy is fit by polynomial function.

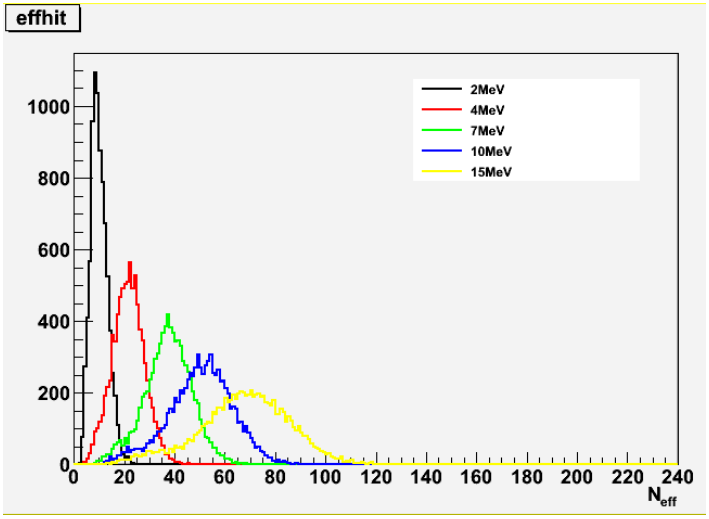

Figure 32: N_{eff} comparison of incident electrons with various energy. It is made by MC simulation.

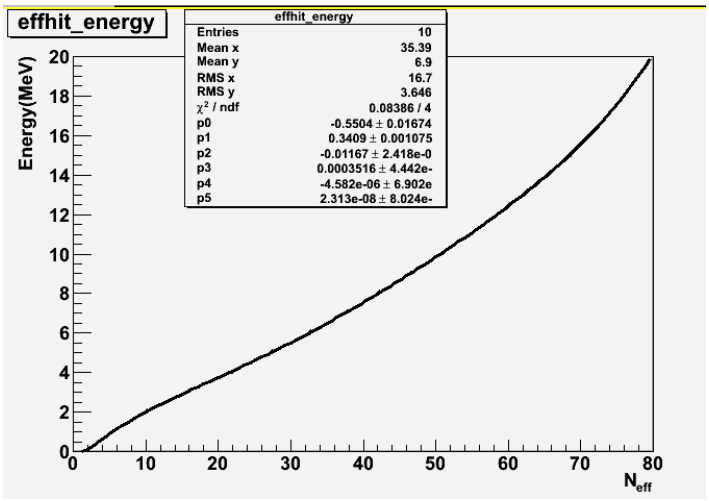

Figure 33: Fitting the relationship of N_{eff} and energy by polynomial function

4.1.4 Monte Carlo tuning

Monte Carlo simulation program of EGADS detector is based on Geant4.9.6p02. Geant4 is a scientific toolkit developed by CERN, it offers a framework for high energy physics simulation. The simulation program of EGADS is called EGSIM, while the official version of Super-K simulation program is called SKDETSIM. EGSIM was developed on the base of SKDETSIM, it redefines the detector and PMTs, and simulates the neutron capture process by gadolinium and protons in 0.2% gadolinium water. The performance of Cherenkov photon in water depends on its wavelength. There are three processes: Rayleigh scattering, Mie scattering, and absorption. The water transparency of 0.2% gadolinium water is measured by spectrometer and has already be inputted into EGSIM. However, it is hard to know how much of the undetected photons are due to absorption and how much of them are due to scattering. We have designed a laser for Rayleigh scattering measurement and the experiment is still in progress. Currently, we determine the parameters by assuming 90% absorption and 10% scattering.

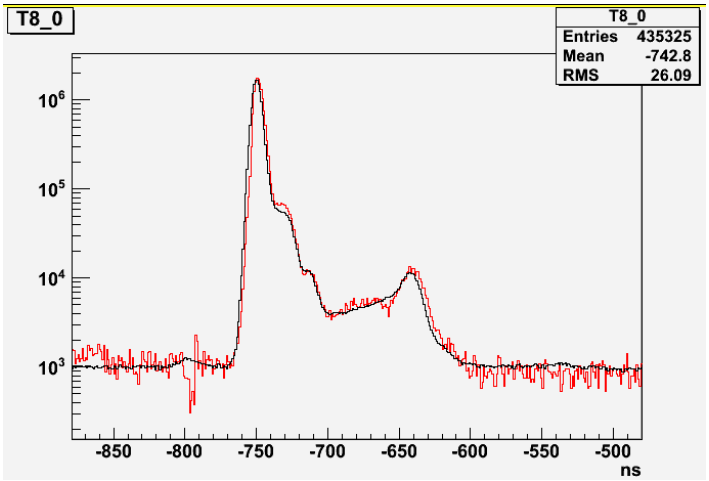

Figure 34: Timing comparison of Data& MC in pure water

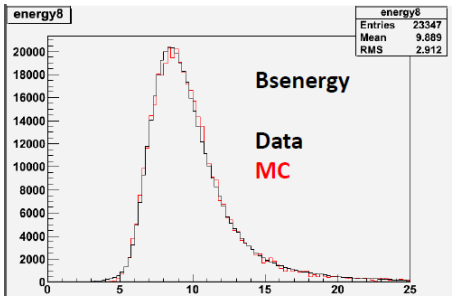

Figure 35: Reconstruction energy of Data& MC in pure water

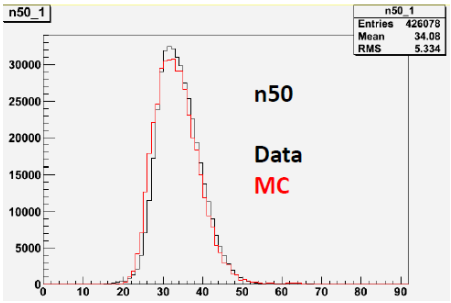

Figure 36: N_{50} of data&MC

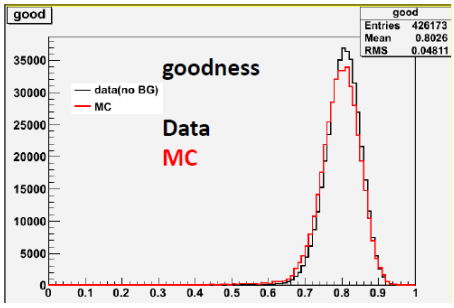

Figure 37: Goodness of Data&MC in pure water. The definition of goodness can be found in previous session.

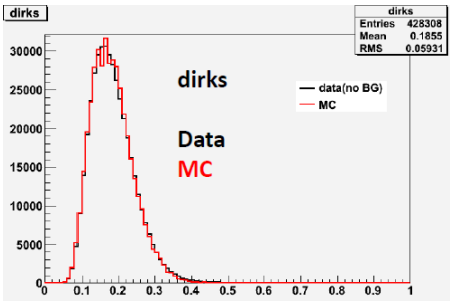

Figure 38: Dirks of Data&MC in pure water. Dirks is a value used to estimate the fitting precision of event direction.

Other calibration results, such as charge distribution of single photon, QE and gain of PMTs, are also inputted. Dark rate and after-pulse of PMTs are finally tuned by Ni-Cf source which is also used for relative QE measurement,

because the signals from Ni-Cf source have a comparatively simple performance in water. Figure above shows the comparison of Ni-Cf data and EGSIM simulation results. After MC tuning, now data and MC have good agreement.

4.2 Estimation of neutron capture efficiency

4.2.1 Detection setup

The most important point of SK-Gd project is the detection of ∼8MeV gamma from neutron capture on gadolinium. In order to estimate the neutron capture efficiency of gadolinium in EGADS, Am/Be are chosen as a neutron source. ^{241}Am decays to ^{237}Np by giving out a ^{4}He, then ^{9}Be reacts with ^{4}He and finally a neutron and a 4.4MeV gamma ray are produced. As mentioned before, in SRN detection events are expected to have two signals, the prompt one is the Cherenkov light made by positron, and the delayed one is the gamma ray made by neutron capture. To make similar events as SRN, Am/Be source is placed on the top of BGO crystal, and the 4.4MeV gamma from Am/Be source can hit on BGO and make scintillation light. The scintillation light made by 4.4MeV gamma has a large number of PMT hits and can be easily separated from neutron capture gamma. By such setting, the scintillation events can be considered as the prompt signal while the neutron capture gamma is the delayed signal, and neutron capture efficiency can be estimated by coincidence detection of these two.

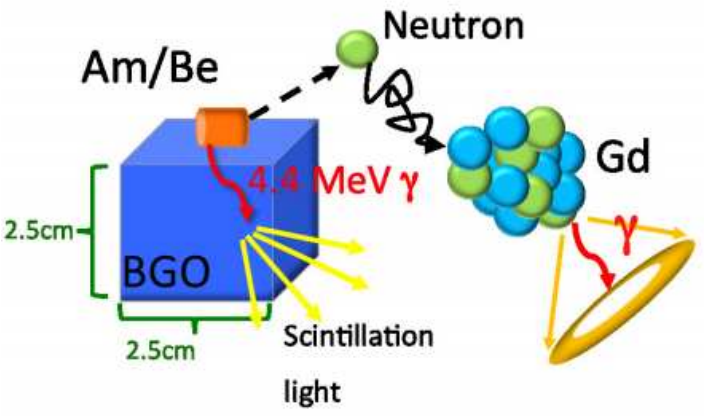

Figure 39: Measurement setup of Am/Be experiment

4.2.2 Data reduction

Before comparing data to Monte Carlo simulation, we should first consider how to remove the background events in data. Scintillation light produced by BGO was found to be too bright that almost all of 240 EGADS PMTs will be hit and it may cause a lot of afterglow events. To reduce the intensity of scintillation light, we cover a kind of black polyethylene terephthalate sheets. The black sheet is opened with several holes to make the scintillation light hit a proper number of PMTs. Figure 40 shows the PMT hit timing distribution of prompt events. As can be seen, there are two peaks in this distribution. First we must

ensure all of these events are all real prompt events produced by 4.4MeV gamma rays and BGO. Figure 40 shows the different performance of Cherenkov light and scintillation light in PMT timing distribution. As can be seen, obviously Cherenkov signal has a much sharper shape than scintillation signal. The N_{30} and N_{400} distribution of prompt events is also in Figure 40. The points around ($N_{30} = 20$,$N_{400} = 80$) are from scintillation light, and the points around ($N_{30} = 40$,$N_{400} = 40$) can be considered to be Cherenkov background events. Therefore, to check if these events are scintillation light emitted by BGO, we calculated the ratio of N_{30} and N_{400} of all the prompt events. A cut of $N_{30}/N_{400} > 2.0$ is applied to remove the Cherenkov background in prompt events. These Cherenkov prompt events are from cosmic muon or gamma backgrounds.

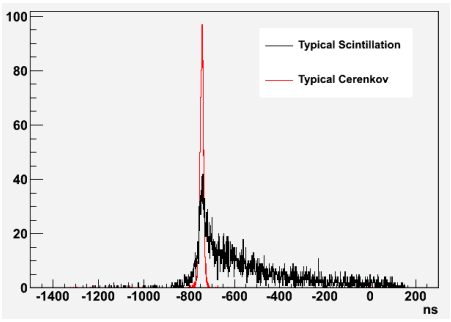

Figure 40: Timing distribution of typical Cherenkov event and typical scintillation event

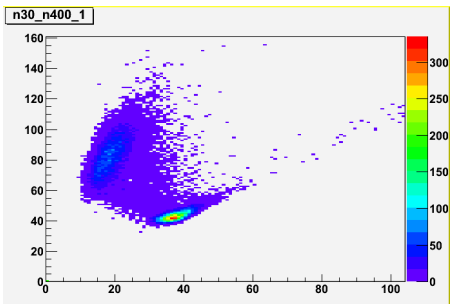

Figure 41: N_{30} and N_{400} of prompt events. Horizontal axis is N_{30} and vertical axis the N_{400}.

Delayed events are applied with reduction. The events with low reconstruction precision($goodness < 0.4$, $dirks < 0.1$, $dirks > 0.4$) are removed. And we select the events which are reconstructed in 2m distance from the tank centre, because the events near the PMT surface have high possibility to be background. After these so-called "precut", the time difference between the delayed events and their corresponding prompt events in 0.2% Gd concentration are shown in Figure 44. The distribution of neutron capture events by Gd follows exponential function and the flat component after 300ns is due to background because the background events do not have relationship with the parent prompt event so they perform to be random.

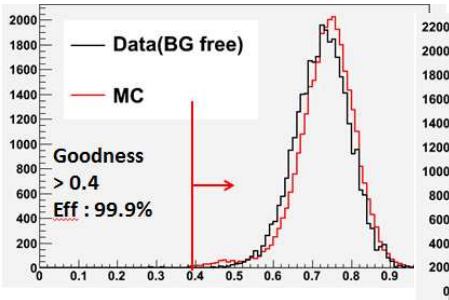

Figure 42: Event cutting for goodness.

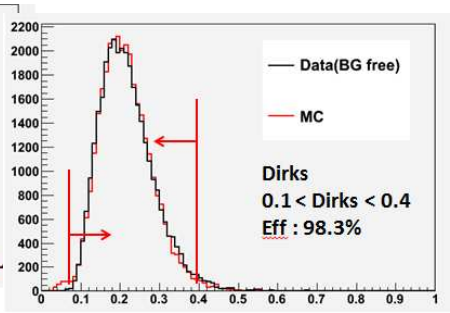

Figure 43: Event cutting for dirks.

The background in delayed events can be considered to be from the environment and the Am/Be source itself. The former one includes both neutrons and gamma rays from environment, and the latter one means the 4.4MeV gamma rays and neutron capture events from the source come into the 1ms gate, even though they are not related to the prompt event which produced the 1ms gate. An efficient method can be used to remove all these backgrounds in delayed events. First we define the events in 0∼500ns in Figure 44 to be on-time events, and relatively define the events in 500∼1000ns to be off-time events. Then background free distribution could be obtained by subtracting off-time events from on-time events.

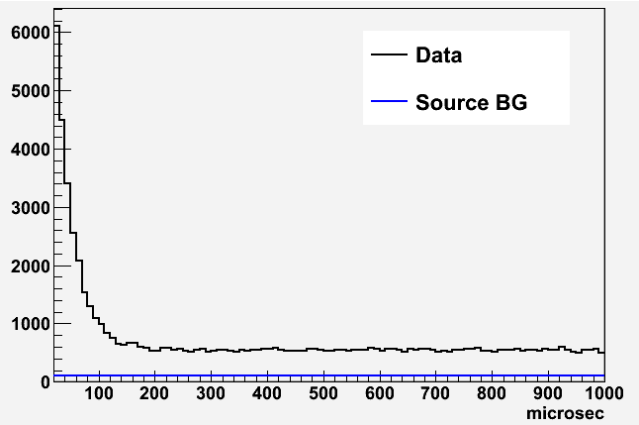

Figure 44: Time difference between prompt event and deleyed events. The blue line is the expect number of the background from the source itself.

When the backgrounds are removed, data is compared with the results of Monte Carlo simulation. As mentioned before, the parameters in Monte Carlo simulation are tuned by Ni-Cf source in pure water. As shown in Figure 45 and Figure 46, the time difference and reconstructed energy of data and Monte Carlo simulation have good agreement. If we fit the distribution of time difference by exponential function as shown in Equation (18), we can obtain the average life time of the neutron in Gd water. Table 3 shows the neutron life time in different Gd concentration, the results are also in anticipation.

$$f(x) = p_0 \times e^{\frac{-x}{p_1}} + p_2 \tag{26}$$

	$2178 \pm 44ppm$	$1055 \pm 21ppm$	$225 \pm 5ppm$
Data	$29.89 \pm 0.33\mu s$	$51.48 \pm 0.52\mu s$	$130.1 \pm 1.7\mu s$
MC	$30.03 \pm 0.77\mu s$	$53.45 \pm 1.19\mu s$	$126.2 \pm 2.0\mu s$

Table 3: Cherenkov threshold for charged particles in water.

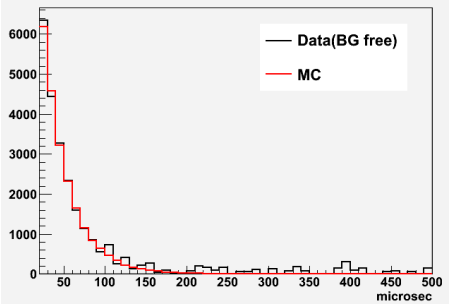

Figure 45: Time difference between prompt and delayed signals.

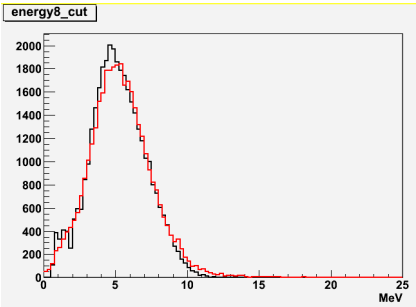

Figure 46: Reconstrued energy of delayed signals.

4.2.3 Fake prompt event

If we count the number of prompt events and delayed events, we found that parts of the prompt events are not followed with its daughter event. When we estimate the neutron capture efficiency and detection efficiency of our detector, we should take such fake prompt events into consideration. The reason for fake prompt has been understood. Very little of them are from environment, while most of them are due to Gd(n,γ). Neutron captured by Gd will produce gamma rays with a total energy of $\sim$8MeV, these gamma rays may hit on the BGO and make scintillation light. If the parent 4.4MeV failed to make prompt trigger, then the scintillation light made by Gd(n,γ) will be recorded as prompt event. This is the main component of fake prompt events. The effect from environment is also measured by the same experiment setup except that the Am/Be source was taken away. The result shows that the fake prompt from environment is about 8 events per hour and it is quite less when compared to the number produced by Gd(n,γ).

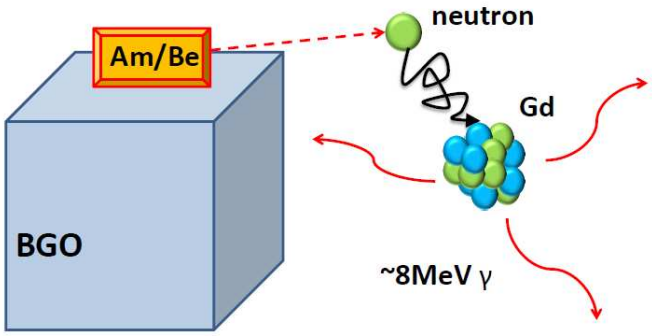

Figure 47: Explanation of the reason of fake prompt events

Since fake prompt events are almost caused by Gd(n,γ), we can estimate it from the Gd(n,γ) events which we already have. Here we select the events which are tagged with both prompt and delayed trigger. That means, these events are inside the 1ms gate which is generated by the parent prompt events, but they exceed the threshold of prompt trigger. Figure 48 shows the time difference between double triggered event and its parent prompt event. Fitting the distribution with exponential function, the average time turns to be $30.11 \pm 0.74 \mu s$ and it is consistent with the neutron life time in 0.2% Gd water which is shown in the previous section. To remove the flat part in this distribution, we can use the on-off method stated before and then we can got the double triggered events which are really caused by Gd(n,γ) and they are free of backgrounds.

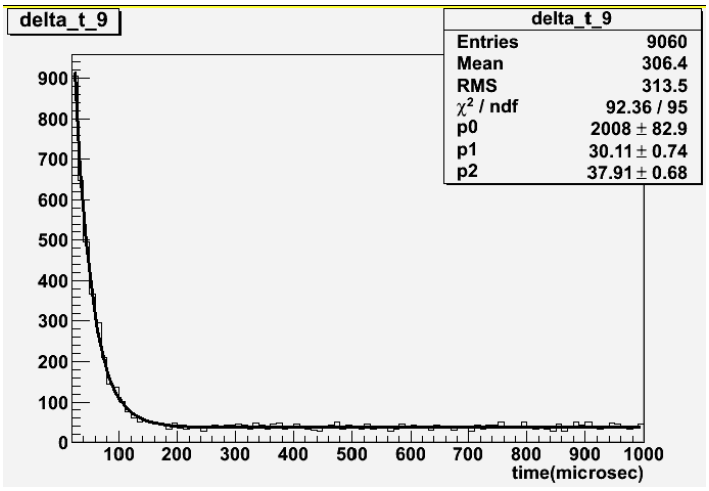

Figure 48: Time difference between the prompt&delayed double triggered events and their parent prompt events.

Figure 47 shows the comparison of prompt events and the prompt&delayed double triggered events which are made from on-off method. Prompt event has two peaks in its distribution, and the distribution of double triggered event is consistent with one of them. Double triggered event has a low ratio of N_{400} over N_{30}, because even if one of the Gd(n,γ) hit on BGO the others will still perform

	$lifetime(\mu s)$
Neutron in 0.2% Gd	$29.89 \pm 0.33 \mu s$
Fake prompt	$30.11 \pm 0.74 \mu s$

Table 4: Cherenkov threshold for charged particles in water.

as Cherenkov light. Normalize the distributions with areas between 0∼60hits, then apply the prompt cut as the last section did, and the proportion of fake prompt events after reduction is 10.02%.

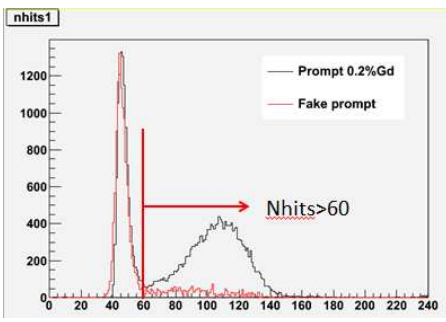

Figure 49: Applying N_{hit} cut onto the prompt&delayed double triggered events

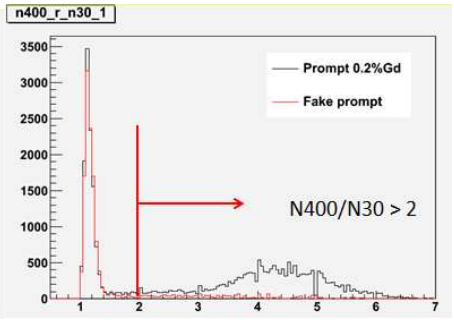

Figure 50: Applying N_{400}/N_{30} cut onto the prompt&delayed double triggered events

4.2.4 Neutron capture efficiency

The purpose of Am/Be experiment is to calculate the neutron capture efficiency and to make sure it is consistent with our expectation. However, when we detect a neutron signal, we do not know whether it is from neutron capture on Gd, or neutron capture on proton or something else. The only to estimate it is to use MC simulation because in simulation program we can know which event is from Gd(n,γ) and which one is not. The Figure 51 shows the N_{50} distribution of MC simulation.

	Data	MC
$Eff_{Gdcapture}$	$84.36 \pm 1.79\%$	$84.51 \pm 0.33\%$

Table 5: Cherenkov threshold for charged particles in water.

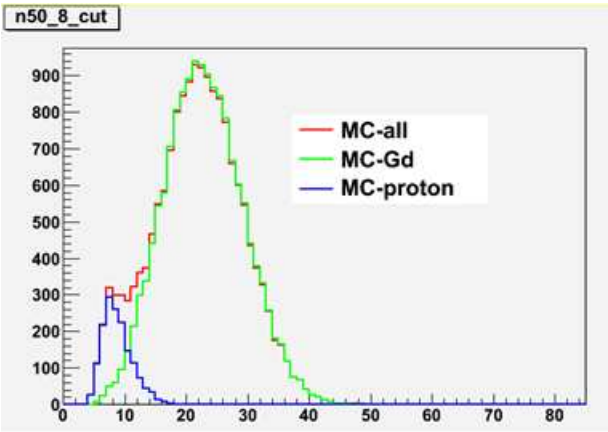

Figure 51: N_{50} of the simulation result. Different colour shows the different component

As can be seen from the Figure, the proton capture component decreases to zero around 4MeV. Here we cut the energy by 4.5MeV and the remaining events are all Gd(n,γ). We can calculate the neutron capture efficiency as follows:

$$N_{prompt} \times Eff_{Gdcapture} \times Eff_{cut(Gd)} = N_{on-off} \tag{27}$$

Here N_{prompt} is the number of prompt trigger. If we consider that one prompt event should be followed by a corresponding neutron event, then N_{prompt} represents the number of neutrons generated from the source. $Eff_{Gdcapture}$ is the neutron capture efficiency which we want to obtain, and $Eff_{cut(Gd)}$ is the analysis efficiency by applying 4.5MeV cut as well as the precut onto the Gd(n,γ) events in MC simulation. N_{on-off} is the number of delayed events after cutting. And finally after considering 10.02% fake prompt, the neutron capture efficiency by Gd is shown in Table 5. The result from real data is consistent with expectation.

5 Summary and prospect

In this thesis, basic overview of Super-K detector and details about SK-Gd project were demonstrated.
To test the Gd effect to Super-K tank, EGADS detector and its own system has been built. 0.2% gadolinium sulfate has already been successfully dissolved into EGADS tank. Water system and transparency measurement device and DAQ electronics are running as expected. Basic calibration work was finished in pure water condition. The measurement of Gd(n,γ) was conducted with Am/Be source, and neutron capture efficiency of gadolinium in EGADS has been estimated.
Based on the success of EGADS, SK-Gd project has already been approved by SK collaboration, with the precise timeline yet to be determined as there are still some remaining works in EGADS.
One thing is Ra/Rn removing. Ra is the impurity in water and Rn is the daughter nuclear produced in the chain decay of Ra. Both of them have radioactivity and will be a neutron background for SRN detection. Now Ra/Rn removing system is being developed in EGADS lab.
Another thing is the update work of electronics. Now the electronics in EGADS is using Analog Timing Module (ATM), which was also used in Super-K first, second and third phase. Super-K fourth phase is using a different one called QTC-Based Electronics with Ethernet (QBEE) because nearby supernova burst will have a extremely high data rate and high performance computing modules are needed. EGADS electronics will be replaced with QBEE in the future to have a completely same condition with Super-K.
In parallel, a GPS timing module and a real-time intelligent trigger system comprised of custom hardware and software will be added, and they are designed to extract the most detailed, accurate supernova neutrino data possible as rapidly as possible.
Once the remaining works in EGADS is finished, we will be prepared to add gadolinium into Super-K.

References

[1] K.Hirata et al. Phys. Rev. Lett. **58**, 1490

[2] R.M. Bionta et al. Phys. Rev. Lett. **58**, 1494

[3] E.Cappellaro, R.Evans, and M.Turatto, Astron. Astrophys. **351**, 459 (1999).

[4] G.S.Bisnovatyi-kogan and Z.F.Seidov, Ann. N.Y. Acad. Sci. **422**, 319 (1984).

[5] T.Totani and K.Sato, Astropart. Phys. **3**,367 (1995)

[6] T.Totani, K.Sato and Y.Yoshii, Astrophys. J. **460**,303 (1996)

[7] R.A.Malaney, Astropart. Phys. **7**125 (1997)

[8] D.H.Hartmann and S.E.Woosley, Astropart. Phys. **7**,137 (1997)

[9] M.Kaplinghat, G.Steigman, and T.P.Walker, Phys. Rev. D **62**, 043001 (2000)

[10] S.Anto, K.Sato, and T.Totani, Astropart. Phys. **18**307 (2003)

[11] Y.Fukuda et al. (Super-Kamiokande Collaboration) 2003 Nuclear Instruments and Methods in Physics Research Section A vol **501** pp418-462

[12] S.Fukuda et al. (Super-Kamiokande Collaboration) 2002 Phys. Lett. B **539** 179

[13] Y.Fukuda et al. (Super-Kamiokande Collaboration) 1998 Phys. Rev. Lett. **81** 1562

[14] K.Abe et al. (T2K Collaboration) 2011 Phys. Rev. Lett. **107** 041801

[15] M.Ikeda, Master Thesis, Okayama University (2007)

[16] J.Beacom and M.Vagins, 2004 Phys. Rev. Lett. **93** 171101

[17] K.Abe et al. (Super-Kamiokande Collaboration) 2014 Nuclear Instruments and Methods in Physics Research Section A vol **737** pp 253-272

[18] S.Ueno, Master Thesis, University of Tokyo (2009)

[19] T.Mori, PhD Thesis, Okayama University (2015)

[20] Y.Koshio, PhD Thesis, University of Tokyo (1998)